EARTH SURFACE PROCESSES AND LANDFORMS
Earth Surf. Process. Landforms **46**, 490–503 (2021)

Published online 17 January 2021 in Wiley Online Library
(wileyonlinelibrary.com) DOI: 10.1002/esp.5041

Observations on decadal sandbar behaviour along a large-scale curved shoreline

R. Gijsman,[1,2]* B.G. Ruessink,[3] J. Visscher[1] and T. Schlurmann[1]
[1] Ludwig Franzius Institute of Hydraulic, Estuarine and Coastal Engineering, Faculty of Civil Engineering and Geodetic Science, Leibniz University Hannover, Hannover, Germany
[2] Marine and Fluvial Systems, Faculty of Engineering Technology, University of Twente, Enschede, Netherlands
[3] Department of Physical Geography, Faculty of Geosciences, Utrecht University, Utrecht, Netherlands

Received 29 May 2020; Revised 20 November 2020; Accepted 23 November 2020

*Correspondence to: Rik Gijsman, P.O. Box 217, 7500 AE Enschede, Netherlands. E-mail: r.gijsman@utwente.nl

ESPL
Earth Surface Processes and Landforms

ABSTRACT: Nearshore sandbars are characteristic features of sandy surf zones and have been observed with a variety of geometries in cross-shore (e.g. location) and longshore direction (e.g. planform). Although the behaviour of sandbars has been studied extensively on spatial scales up to kilometres and timescales up to years, it remains challenging to observe and explain their behaviour on larger spatial and temporal scales, especially in locations where coastline curvature can be prominent. In this paper, we study a data set with 38 years of coastal profiles, collected with alongshore intervals of 50 m, along the 34 km-long curved sandy shoreline of Sylt island, Germany. Sylt's shoreline has an orientation difference of ~20° between the northern and southern half of the island. We found that the decadal coastal profiles on the southern half show features of a low-tide terrace and a sandbar located further from the shoreline (~441 m). On the nothern half, the sandbar was located closer to the shoreline (~267 m) and was less pronounced, while the profiles show transverse bar and rip features. The alongshore planform also differed systematically and significantly along the two island sides. The sandbar on the southern island half, with alongshore periodicity on a larger length scale (~2240 m), was coupled out-of-phase to the shoreline, while no phase coupling was observed for the sandbar with periodicity on a shorter length scale (~670 m) on the northern half. We related the observed geometric differences of the sandbars to the difference in the local wave climate along Sylt, imposed by the shoreline shape. Our observations imply that small alongshore variations in wave climate, due to the increasing shoreline curvature on larger spatial scales, can lead to significant alongshore differences in the decadal evolution of coastal profiles, sandbars and shorelines. © 2020 The Authors. Earth Surface Processes and Landforms published by John Wiley & Sons Ltd

KEYWORDS: alongshore variability; coastal profiles; curved coastlines; nearshore morphology; nearshore sandbars; sandbar–shoreline coupling

Introduction

Shoreline parallel sand ridges, or nearshore sandbars, often frame as crescentic plan shapes with alongshore periodicity in cross-shore location and depth. These crescentic sandbars are characteristic of many surf zones of wave-dominated sandy beaches and their alongshore periodicity, three-dimensionality, or 3D length scale has been observed to vary from 100 to 3000 m along different individual stretches of shoreline worldwide (Van Enckevort and Ruessink, 2003; Van Enckevort *et al.*, 2004; Ribas *et al.*, 2017).

These sandbars are often coupled to the shoreline. This coupling is also highly site-specific and has been observed out-of-phase (i.e. shoreward-directed shoals face offshore shoreline perturbation) and in-phase (i.e. shoreward-directed shoals face onshore shoreline perturbations) on timescales up to years (Ruessink *et al.*, 2007; Quartel *et al.*, 2008; Van de Lageweg *et al.*, 2013; Athanasiou *et al.*, 2018).

The large-scale and long-term evolution of nearshore sandbars is important for coastal management because sandbars induce depth-limited wave breaking, while sandbar–shoreline coupling can result in alongshore variability in dune erosion (Thornton *et al.*, 2007; Galal and Takewaka, 2011; Castelle *et al.*, 2015). Most existing sandbar (Wright and Short, 1984; Lipmann and Holman, 1990; Van Enckevort and Ruessink, 2003; Splinter *et al.*, 2011) and sandbar–shoreline coupling (Ruessink *et al.*, 2007; Castelle *et al.*, 2010a,b; Price and Ruessink, 2013; Van de Lageweg *et al.*, 2013) studies were, however, limited to individual shorelines, with spatial scales up to kilometres and timescales up to years.

On larger spatial scales, shorelines typically increase in curvature, resulting in an increasing alongshore variability in wave

climate (e.g. wave height and angle of incidence), which can systematically affect the behaviour of sandbars and shorelines on the timescale of years (Rutten *et al.*, 2018, 2019). A systematic difference in the interaction between the sandbar, shoreline, hydrodynamic and morphological processes could thus result in significant alongshore variations in the sandbar geometry on longer timescales.

In these previous studies the three-dimensionality of sandbars was generally shown to increase (i.e. from 2D to 3D) during calm conditions with near-zero wave angles, and to decrease (i.e. bar straightening) during energetic wave conditions with higher wave heights (Wright and Short, 1984), or larger wave angles of incidence (Price and Ruessink, 2013), which force a stronger alongshore current and sediment transport rate. With near-zero angles or moderately oblique waves, the wave angle of incidence was also found able to cause growth of the sandbar three-dimensionality (Calvete *et al.*, 2005; Rutten *et al.*, 2018). Moreover, along the curved coastline of the Sand Engine in the Netherlands, the three-dimensionality of the sandbar increased gradually during calm conditions with near-zero wave angle on the northern side, but on the western side the sandbar three-dimensionality grew rapidly during more energetic conditions with a larger wave angle of incidence (Rutten *et al.*, 2018).

The degree of phase coupling between sandbar and shoreline is, according to the beach state model of Wright and Short (1984), dependent on their separation distance. This suggestion was confirmed with field observations (Van de Lageweg *et al.*, 2013; Athanasiou *et al.*, 2018; amongst others). An out-of-phase coupled sandbar–shoreline was typically explained by the dominant effect of the cross-shore wave-breaking location induced by the water depth variability along the sandbar (Coco and Murray, 2007; Castelle *et al.*, 2010a; Coco *et al.*, 2020). The resulting alongshore varying wave height and wave setup provoke a horizontal recirculation cell at the shoreline. The morphological evolution of the sandbar and shoreline is then governed by the positive feedback between hydrodynamic and sediment transport processes as well as evolving morphology (Falques *et al.*, 2000). Furthermore, wave angles also affect the phase of the coupling between sandbar and shoreline (Price and Ruessink, 2013; Price *et al.*, 2014), since increased angles of wave incidence can create meandering longshore currents between the shoreline and the sandbar. This process, in turn, affects the horizontal

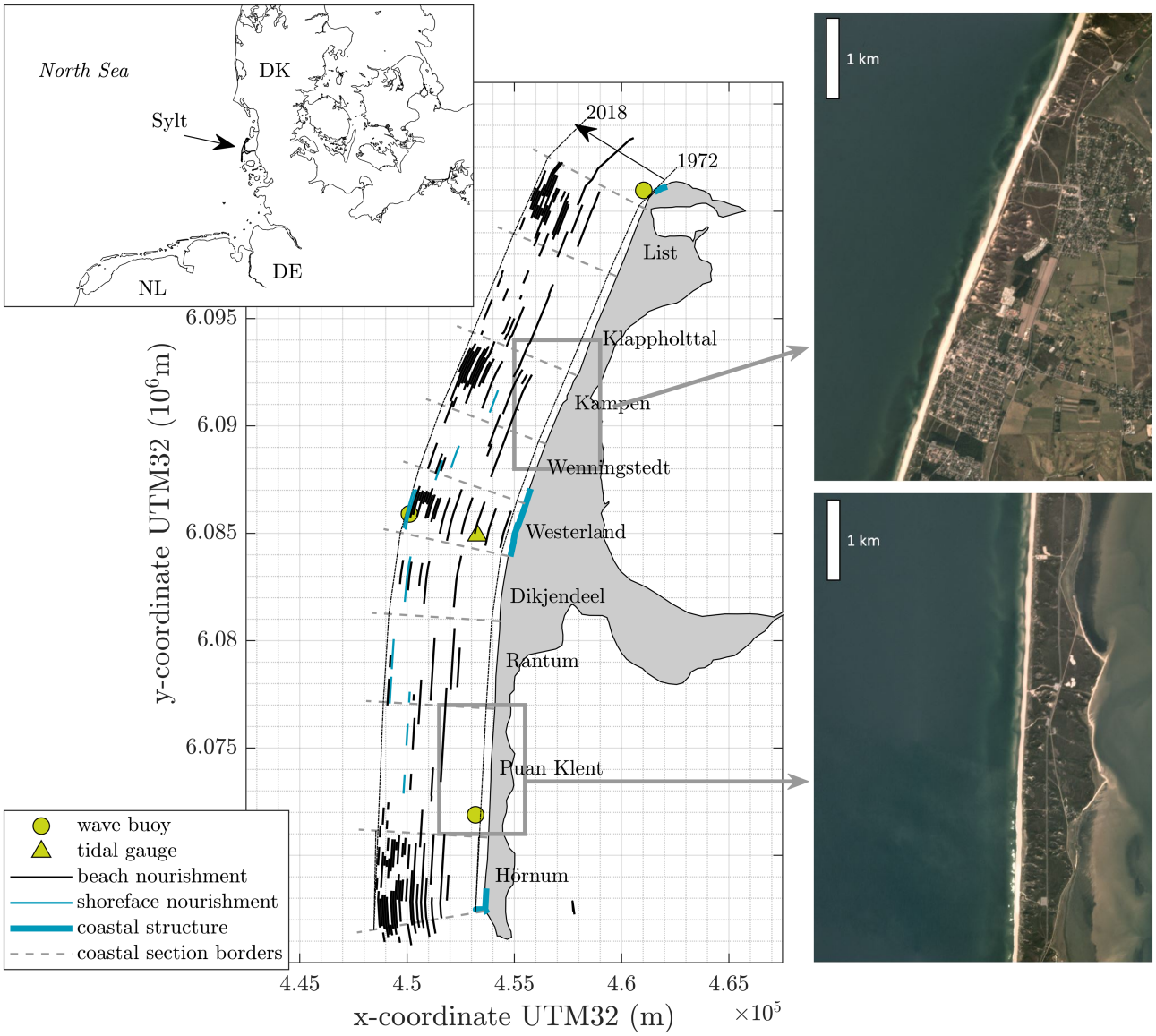

Figure 1. The island of Sylt in Germany (inset left). Coastal structures (thick blue lines) and sand nourishments on beach (black lines) and in the shoreface (blue lines) have been constructed in the last century to mitigate the effects of coastal erosion (distance from the shoreline indicates timing of the nourishment). From aerial images it can already be observed that the sandbar geometry differs along Sylt (inset right). Aerial images of August 2019 were extracted from planet.com. [Colour figure can be viewed at wileyonlinelibrary.com]

recirculation cells and leads to the in-phase coupling of the sandbar and the shoreline.

Although the complex morphological evolution and coupling of sandbars and shorelines has been studied extensively, it remains challenging to explain the considerable variations in observed sandbar geometry and how these result from interactions between hydrodynamic and morphological processes. In this study, we analyse a data set with 38 years of beach profiles measured along the 34 km-long island of Sylt. Sylt's west coast has an orientation difference of approximately 20° between the northern and southern half (Figure 1). We describe and compare the decadal evolution of the sandbars along both sides in relation to the small difference in local wave climate that is imposed by the shoreline curvature. In this way, we aim to gain more insight in the sensitivity of sandbar and shoreline behaviour to shoreline curvature.

This paper is organized as follows. We first describe the field study site, the characteristics of the data set and the analysis procedure. Thereafter, we present the decadal behaviour of both shoreline and sandbar, including their coupling and the sandbars' response to an engineering intervention (shoreface nourishment). In the discussion, we hypothesize how the observed behaviour of the sandbar has been affected by the interaction between the sandbar, the shoreline, hydrodynamic and morphological processes along the two island sides, before we present the main conclusions of this work.

Methodology

Study site and data

Sylt, an iconic tourist destination in Germany, is the country's northernmost Wadden Sea barrier island and was the field site of this study (Figure 1). The shoreline of Sylt suffers from severe coastal erosion and is heavily engineered by means of coastal structures and artificial sand nourishments on its beaches (i.e. beach nourishments) and in the shoreface (i.e. shoreface nourishments), see Figure 1 (Gijsman *et al.*, 2019; Staudt *et al.*, 2019). Sylt's west coast consists of medium sand with a D_{50} of approximately 360 µm (Mielck, 2017) and has an alongshore length of approximately 34 km. With respect to the north, its orientation ranges from 2° (in the south) to 22° (in the north). The convex shape of the island resulted in time-averaged southward (northward) longshore sediment transport rates on the southern (northern) half. Based on shoreline retreat rates between 1876 and 1997, approximately 0.5 and 1 Mm^3 were lost yearly on the southern and northern half of Sylt, respectively (Dette, 1998; Ahrendt, 2001; Kroon *et al.*, 2007).

To counteract the severe erosion, seawalls were constructed in Westerland and List, and a tetrapod groin in Hörnum (Figure 1). Thereafter, nourishments were placed regularly since 1972 and on an annual basis since 1983. On average, 3.34 nourishments were placed per year with a total yearly volume of approximately 1.0 Mm^3 (average of 316 000 m^3 per nourishment). The nourishment focus was specifically on the erosion hotspots in the centre (Westerland and Kampen) and at both ends (Hörnum and List) of the island. Due to the larger erosion volumes, the nourished volumes on the northern half exceed those on the southern half.

A tidal gauge and a directional wave buoy (LKN.SH, 2016b) were located at 2 and 5 km offshore Westerland in water depths of 10 and 13 m, respectively (Figure 1). Mean tidal ranges vary between 2.0 and 1.8 m during a spring–neap tidal cycle (Ahrendt and Koester, 1996; Blossier *et al.*, 2016). Tidal currents typically vary between 0.1 and 0.3 $m\,s^{-1}$ and sometimes increase up to 1 $m\,s^{-1}$ in the nearshore (LKN.SH, 2016b). Median wave direction in Sylt is 273° relative to the north (Figure 2a). Between 1998 and 2018, the 50th percentile and 90th percentile of the recorded spectral wave height (H_{m0}) were 0.83 and 1.91 m. For the recorded peak wave period (T_p) these values were 6.1 and 10.8 s, respectively. During winter, more energetic waves generally approach from a westerly to south-westerly direction (Figure 2c). During summer, moderate waves approach from a westerly to north-westerly direction (Figure 2b).

Bathymetric measurements were carried out along the shoreline of Sylt by means of beach profiles. The emerged part of the beach profile was measured with RTK-GPS and LiDAR measurements [O(1 cm) accuracy], the submerged part with echo-sounding measurements [O(10 cm) accuracy]. In Westerland, regular surveys started after the first nourishment campaign of 1972. In the 1980s, measurements initiated along the complete shoreline, with a total of 691 transects. The transects were evenly distributed with mean spatial intervals Δy of 50 m. Coordinate y was defined along the shoreline, increased from south to north and was equal to 0 m in front of Westerland. Between 1980 and 2018, an average of 53.9 measurements (σ = 16.6) were collected per transect. Timing and location of the measurements were related to the nourishment activities. The data set therefore consisted of measurements

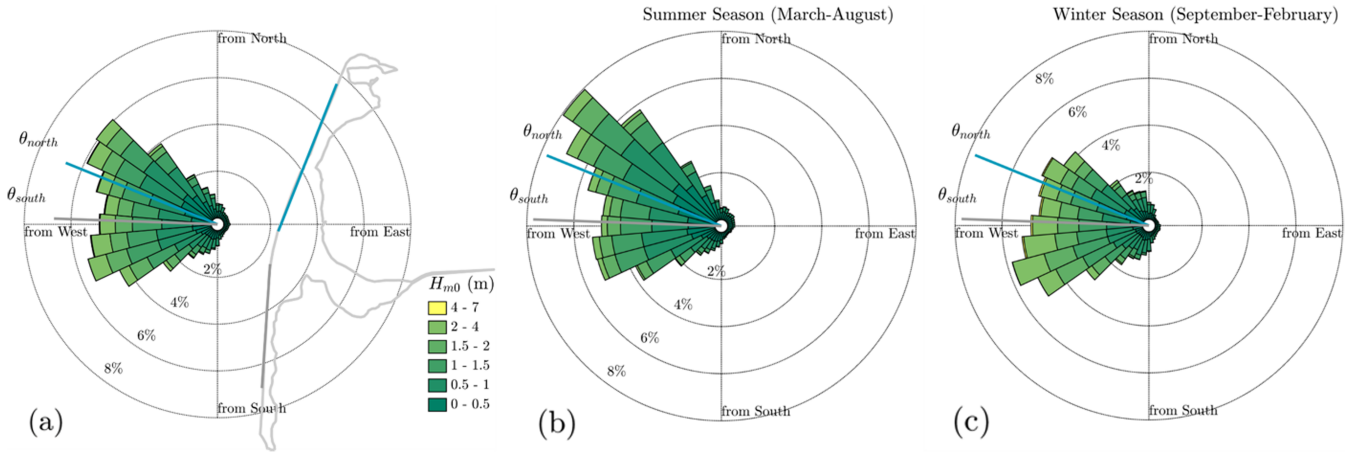

Figure 2. Wave roses from the Westerland wave buoy between 1988 and 2018 during (a) the full year, (b) the summer season and (c) the winter season. The grey and blue lines indicate the shoreline angles of the southern and northern half of Sylt. [Colour figure can be viewed at wileyonlinelibrary.com]

Table 1. Definition of coastal profile areas and mean and standard deviation slope of the reference topography/bathymetry for the southern half ($y < 0$) and northern half ($y > 0$) of Sylt

Area name	Cross-shore distance	Slope south	Slope north
Dune	$x_{z=8} < x < x_{z=4}$	1:4.6 (1:0.9)	1:5.4 (1:1.0)
Beach	$x_{z=4} < x < x_{z=0}$	1:12 (1:1.2)	1:19 (1:1.7)
Upper shoreface	$x_{z=0} < x < x_{z=-3}$	1:67 (1:5.7)	1:55 (1:4.7)
Middle shoreface	$x_{z=-3} < x < x_{z=-5}$	1:175 (1:10)	1:140 (1:20)
Lower shoreface	$x_{z=-5} < x < x_{z=-8}$	1:67 (1:6.7)	1:100 (1:19)

with irregular temporal intervals (Δt), cross-shore extents (∂x) and spatial intervals in cross-shore (Δx) and alongshore (Δy) directions.

Cross-shore location x was defined relative to a time-averaged reference topography/bathymetry, based on the measurements between 1980 and 2018. In the reference, the vertical elevation was equal to zero (z = 0 m) at x = 0 m, and x increased in the offshore direction. The horizontal location of the z = 0 m depth contour was determined with individual measurements that covered the part of the profile between z = −0.5 and 0.5 m and had a maximum spatial interval Δx of 5 m within that area (an average of 18.8 measurements per transect).

The z = 4 and 8 m height contours of the reference topography were determined similarly (average of 26.1 and 21.5 measurements per transect). A larger spatial resolution Δx of 10 m was allowed to determine the z = −3, −5 and −8 m depth contours (average of 14.0, 12.9 and 9.3 measurements per transect). A moving-average filter (bin width ~500 m) was applied to reduce the alongshore variability of the depth contours due to differences in amount and timing of measurements between neighbouring transects. The cross-shore areas between the reference depth contours were defined as characteristic parts of the profile, as presented in Table 1 and Figure 3.

Focus areas

To quantify the behaviour of sandbar and shoreline, the focus was on two shoreline stretches in particular: Kampen, 3.5 km long and located on the northern half of Sylt (y = 4.5 to 8.0 km) and Puan Klent, 6.0 km long and located on the southern half of Sylt (y = −14.1 to −8.1 km), Figure 1. With shoreline orientations of 22 and 2°, respectively relative to the north,

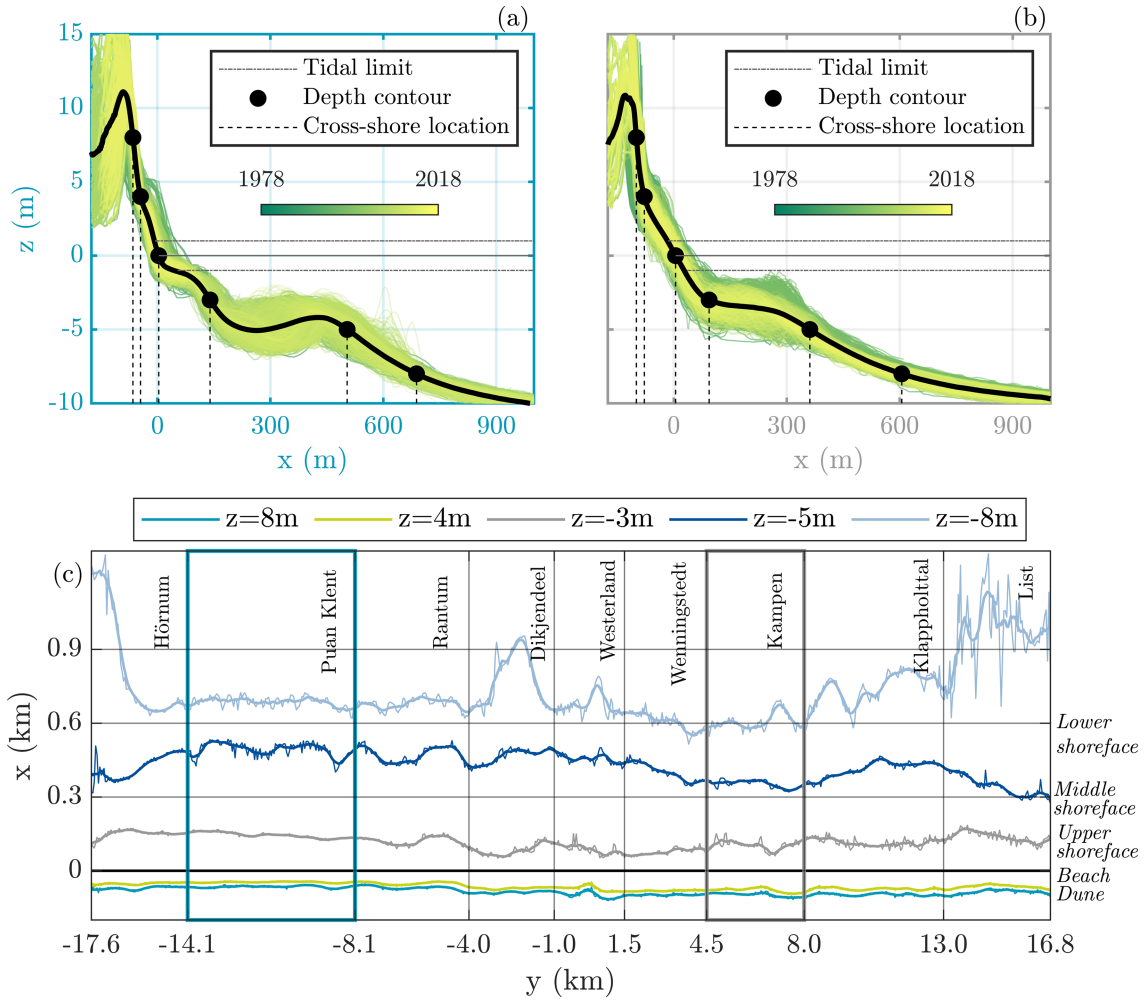

Figure 3. Profile measurements and time-averaged profile (black line) of (a) Puan Klent and (b) Kampen. (c) The time-averaged depth/elevation contours along Sylt, indicating the cross-shore profile areas on the right. A filter was used (thick lines) to reduce the alongshore variability (thin lines). [Colour figure can be viewed at wileyonlinelibrary.com]

Kampen and Puan Klent represent the differences between the northern and southern halves of Sylt (indicated in Figures 3, 4 and 6 by the grey and blue boxes). The temporal evolution of the shoreline and sandbar was assessed for these stretches. Additionally, the monitored response of the sandbars to one of the engineering interventions, a shoreface nourishment, was studied in detail to gain more insight into the short-term behaviour of the sandbars.

In Kampen, the response to the shoreface nourishment placed between 27 April and 11 June 1996 was studied. The shoreface nourishment had a volume of 239 000 m^3 and was constructed at the location of the sandbar. The nourishment had an alongshore length of 1152 m (average 208 m^3 m^{-1}). The nourishment was monitored frequently within the first year after construction, with conducted surveys before (7 April 1996) and after (22 July 1996/19 August 1996/20 September 1996/15 November 1996/20 December 1996/15 March 1997/17 April 1997/1 June 1997/15 August 1997) the nourishment (LKN.SH, 2016a).

In Puan Klent, the response to a double nourishment was studied, which was placed between 15 July and 2 October 2006. The nourishments were placed on the seaside of the sandbar. The nourishments had volumes of 135 000 m^3 (southern) and 391 000 m^3 (northern) (i.e. total of 526 000 m^3) and alongshore lengths of 900 and 1001 m, respectively (i.e. an average of 150 and 391 m^3 m^{-1}). Bathymetric surveys were conducted 1 year before (7 July 2005), during (13 September 2006) and with half-yearly intervals after the construction (13 October 2006/29 March 2007/23 October 2007/15 April 2008/19 January 2010/16 June 2010) (LKN.SH, 2016a).

Studied parameters

The data set was analysed by means of the following parameters:

- sand volumes in different parts of the cross-shore profile (see Table 1);
- cross-shore bar crest locations, depth and amplitude;
- bathymetric measurements;
- wave height and direction;
- longshore sediment transport rate.

Sand volumes in each part of the beach profile were integrated between two horizontal limits and a vertical limit at $z = -10$ m. The horizontal limits depended on the considered part of the profile and were based on depth contours (see Figures 3a and b). Before this calculation, profiles were linearly interpolated on a cross-shore grid with a resolution of 1 m, while profiles with larger cross-shore intervals than 20 m in the relative part of the profile were omitted from the analysis. To determine individual alongshore beach volumes, a moving-average filter (bin width ~400 m) was applied to these volumes in the beach part of the profile.

To determine the cross-shore location of the sandbar crest, the location in the middle shoreface part of the profile with the maximum elevation above a linear fit between the reference $z = 0$ and -8 m depth contours was detected. In this way, an approach as described by Athanasiou *et al.* (2018) was followed. Profiles with maximum horizontal interval Δx of 20 m in the middle shoreface part of the profile were included (average of 19.6 measurements per transect). Continuous alongshore bar crest locations were computed with a moving-average filter (bin width ~400 m).

Alongshore beach volumes and bar crest lines were analysed by their mean and temporal variability. For Kampen and Puan Klent, the alongshore mean and standard deviation of the alongshore beach volumes and bar crest locations were calculated (following Rutten *et al.*, 2018). Length scales of three-dimensionality were determined with a standardized 'find peaks' algorithm based on a threshold amplitude. The algorithm detected the alongshore location of the peak beach volumes and the horns of the bar crest locations. Surveys that covered more than 60% of the coastal transects in the particular stretch were considered in the computation. Shoreline–sandbar coupling was qualitatively assessed by visually comparing the long-term evolution of alongshore beach volumes and bar crest locations. The measurements from which beach volumes and bar crest locations were calculated were mostly not sampled at the same time. The longshore interval and frequency of these measurements also limited a quantitative assessment.

To quantify the response of the sandbars to the shoreface nourishments, measured profiles were linearly interpolated on a grid with longshore grid size of 10 m and cross-shore grid size of 1 m and compared to pre-nourishment conditions. Long- and cross-shore mean differences were analysed to determine long- and cross-shore changes induced by the nourishment (following Huisman *et al.*, 2019). The long- and cross-shore variability were studied with the long- and cross-shore standard deviation. The mean and standard deviation in longshore direction were applied to the complete coastal stretches. Cross-shore limits were set at $x = 0$ and 800 m.

The wave conditions were evaluated by means of hourly spectral wave height ($H_{m0,13}$) and wave direction (Θ_{13}) from the Westerland buoy, located in a water depth of 13 m. To obtain an indication of potential alongshore transport rates, these conditions also served as input for the CERC formulation (CERC, 1984):

$$Q_y = \frac{\rho_w \cdot K \cdot \sqrt{\frac{g}{\gamma_b}}}{16 \cdot (\rho_s - \rho_w) \cdot (1 - p)} \cdot H_{m0,13}{}^{5/2} \cdot \sin(2\theta_{13}) \quad (1)$$

with sand density $\rho_s = 2650$ kg m^{-3}, water density $\rho_w = 1030$ kg m^{-3}, gravitational acceleration coefficient $g = 9.81$ m s^{-1}, empirical coefficient $K = 1$, breaker coefficient $\gamma_b = 0.78$, porosity $p = 0.4$, wave height H_{13} (in metres) and wave angle Θ_{13} (in degrees). Additionally, wave height near the shoreline was calculated assuming full refraction (towards 0°), while shoaling was disregarded:

$$H_n = H_{13} \cdot \sqrt{\frac{\cos(\theta_{13})}{\cos(\theta_n)}} \quad (2)$$

Here, H_n is the wave height near the shoreline and Θ_n the wave angle near the shoreline (= 0°). The long-term wave climate was evaluated with half-year averaged values using a moving-average filter (window of ~182.6 days).

Results

Decadal profile characteristics

The time-averaged depth contours along the island of Sylt varied considerably and, corresponding to the shoreline orientation, a clear separation point was present in the centre of the island (Figure 3c). On the decadal timescale, beach slopes (between the $z = 0$ and 4 m contours) were significantly milder on the northern half of the island (1:19) than on the southern half (1:12). In the middle shoreface (between the $z = -3$ and -5 m contours) the slope was steeper on the northern half

(1:140) than on the southern half (1:175). Table 1 provides more details on the profile slopes and their time-averaged alongshore variability.

The measured profiles in Puan Klent (Figure 3a), on the southern half of Sylt, presented initial erosion on the beach (retreating green lines), which reduced over time. More recent profiles (yellow lines) approached the long-term averaged profile of the coastal section (black line). The profiles showed the decadal presence of a low-tide terrace, in combination with a dynamic Gaussian-shaped nearshore sandbar located further from the shoreline in a larger water depth. In Kampen (Figure 3b), on the northern half of Sylt, the measured profiles also showed initial erosion, especially in the nearshore area. The profiles then approached the time-averaged profile in the coastal section. While the spatial variability on the beach remained larger than in Puan Klent, the nearshore presented a less dynamic and less-pronounced sandbar. The larger variability in the beach part of the profiles resulted from, amongst others, the frequent implementation of beach nourishments.

The time-averaged profiles of Puan Klent and Kampen can be described with an intermediate beach state according to Price and Ruessink (2011). However, the profiles in Puan Klent showed characteristics described by the 'Ridge-Runnel or Low-Tide Terrace' state in combination with an offshore-located 'Rhythmic Bar'. The Kampen profile showed features of the 'Transverse Bar and Rip' state with a wider beach and a less pronounced sandbar. These observations highlight the significant difference in decadal profile characteristics along the curved coast that may affect the morphological behaviour of the sandbar and shoreline, and vice versa.

Large-scale variability in shoreline and sandbar evolution

To illustrate the large-scale evolution of shoreline and sandbar along Sylt, we present the temporal variability of the beach volume (Figure 4), a typical sandbar configuration (Figure 5) and the temporal variability of the bar crest location (Figure 6). The observed alongshore variability in beach width reflected directly on the alongshore variability in beach volume: mean beach volumes on the northern half were significantly larger (895 m^3) than on the southern half (672 m^3).

Figure 4b shows the temporal variability in beach volume at each transect relative to the mean. Increased beach volumes (warm colours in Figure 4b) were present as a result of the beach nourishments that restored eroded profiles (cold colours in Figure 4b), especially in Hörnum (y = −17.6 to −14.1 km), Westerland (y = −1.0 to −1.5 km), Kampen (y = 4.5 to 8.0 km) and List (y = −13.0 to −16.8 km) (see Figure 4b). For more details on the temporal variability in beach volume at Westerland, we refer to Gijsman *et al*. (2019). Furthermore, the variability in beach volumes on the northern and southern half of Sylt differed, with larger variability on the northern half. A closer visual inspection of the data reveals shoreline undulations of O(100 m) on the northern half, for instance between y = 1.5 to 4.5 km and 2000–2010. On the southern half, the data shows shoreline undulations of O(1000 m), for instance between y = −17.6 to −8.1 km and 2000–2018 (Figure 4b). These observations suggest a difference in dominating length of morphological evolution along the curved coastline of Sylt.

A similar difference was present in the subtidal bathymetries, measured on 25 May 1999 and 15 May 2000 (Figures 5a and b). On the northern half, the sandbar planform varied significantly, with smaller length scale of alongshore variability compared to the southern half. On the southern half, Sylt was characterized by a large-scale crescentic sandbar, with wavelength on a larger spatial scale O(1000 m). Figure 5c shows that the morphological changes on the northern half exceeded those of the southern half. Please note that no nourishments were placed between these measurements and bathymetric changes resulted from almost 1 year of hydrodynamic and morphological interactions. In this period, the hydrodynamics were characterized by a relatively stormy winter season, with five events of daily wave height exceeding 3 m (increased up to 4.32 m in January 2000). Time-averaged wave angles of incidence were 3° (southward) on the southern half and −15° (northward) on the northern half in this period.

The cross-shore location of the sandbar crest also differed significantly between the two island sides (Figure 6a). The

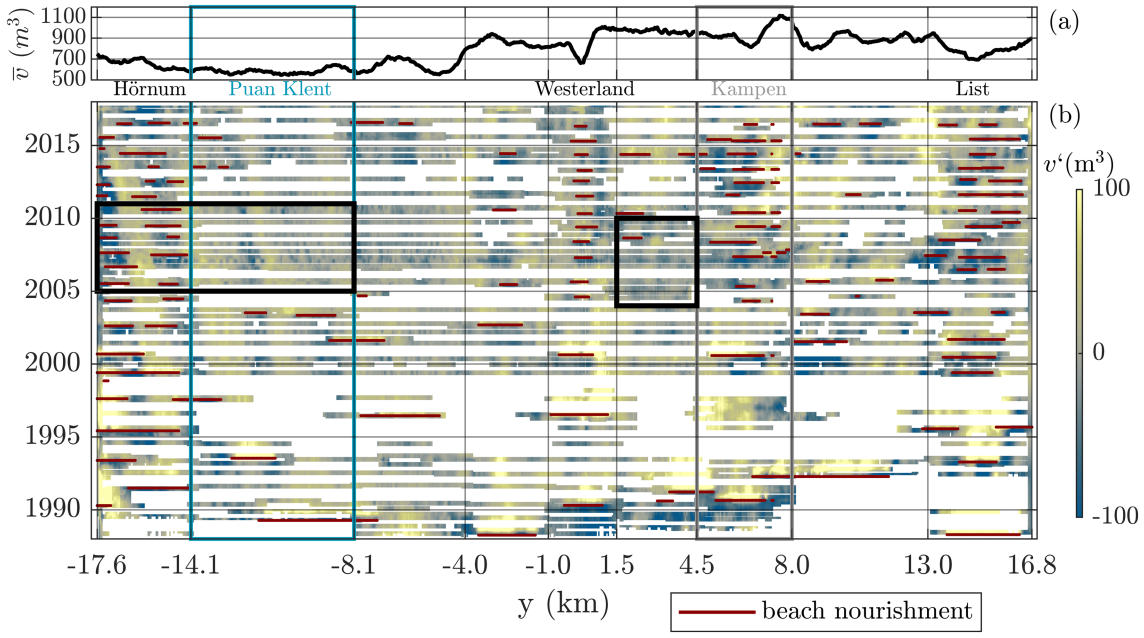

Figure 4. (a) Time-averaged beach volume along Sylt and (b) temporal variability in beach volume relative to the mean. Measurements are linearly spatiotemporally interpolated up to 8 weeks in time and 200 m in space for visualization purposes. Red lines show timing and location of beach nourishments. Boxes to indicate Puan Klent (blue), Kampen (grey) and areas for closer visual inspection (black) are included. [Colour figure can be viewed at wileyonlinelibrary.com]

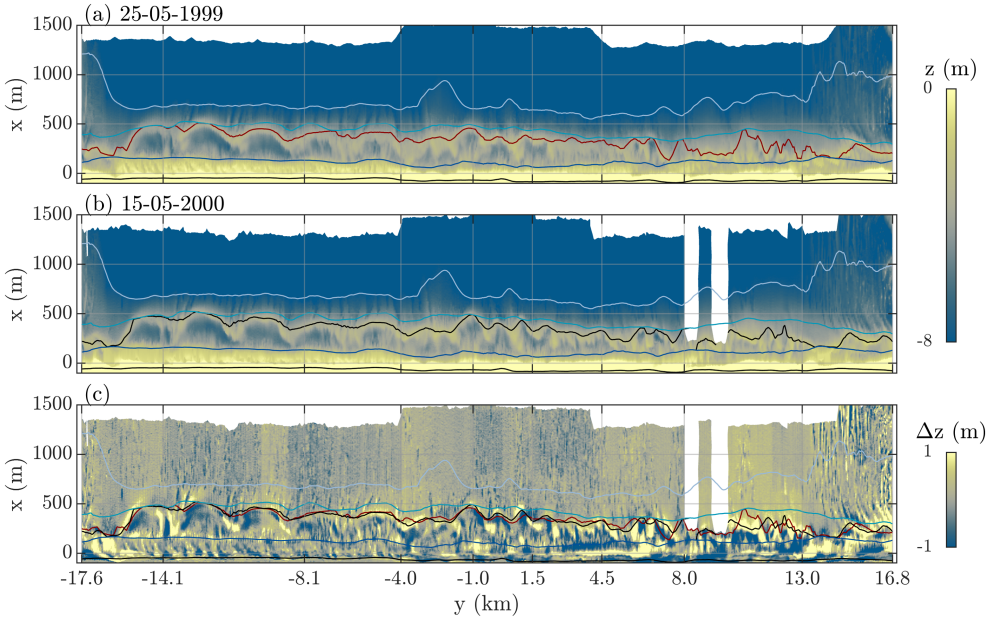

Figure 5. Bathymetry with bar crest location (red line in a, black line in b) of (a) 25 May 1999 and (b) 15 May 2000 and (c) their difference. The yellow (warm) colour indicates an increase in bed level, the blue (cold) colour a bed-level decrease in panel c. Light blue, cyan, blue and black lines in all panels indicate the −8, −5, −3 and 4 m depth contours of the reference bathymetry/topography. [Colour figure can be viewed at wileyonlinelibrary.com]

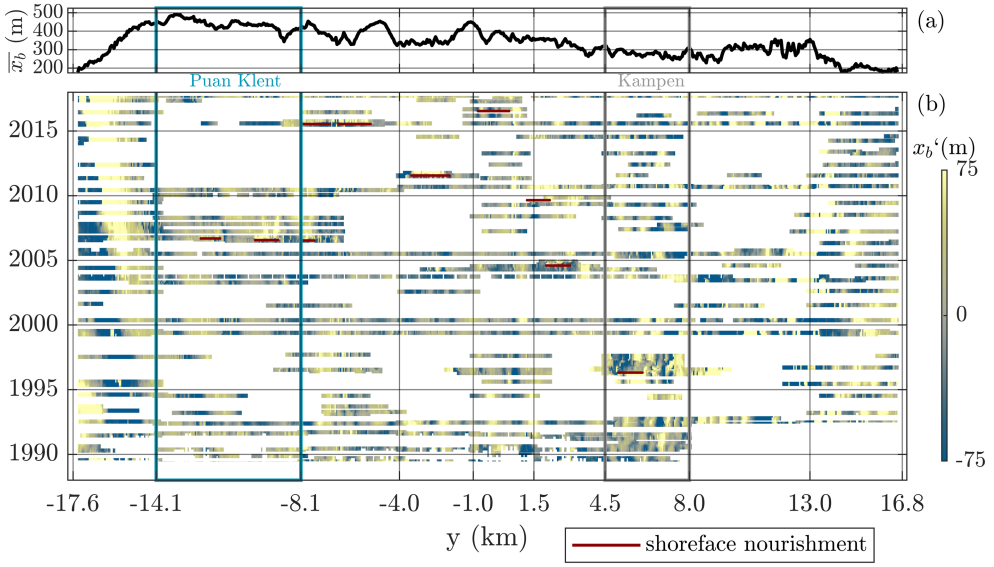

Figure 6. (a) Time-averaged cross-shore bar line location along Sylt and (b) spatiotemporal variability of cross-shore bar line relative to the mean. Measurements are linearly spatiotemporally interpolated up to 8 weeks in time and 200 m in space for visualization purposes. Red lines show timing and location of shoreface nourishments. Puan Klent (blue) and Kampen (grey) beach sections are indicated. [Colour figure can be viewed at wileyonlinelibrary.com]

average bar crest location was smaller on the northern half (268 m) compared to the southern half (357 m). Corresponding time-averaged bar crest depth and amplitude were also smaller, at 3.16 m (compared to 3.37 m) and 0.20 m (compared to 0.97 m). Similar to the observations for the beach volume, the variability in bar crest locations differed between the northern and southern half of Sylt. Their length scales also seem similar to those observed for the beach volumes.

Decadal shoreline – shoreline behaviour

Figures 7a and b show the temporal variations in beach volume and bar crest location for Kampen and Puan Klent specifically. Mean beach volume, cross-shore bar crest location and bar crest depth were 941 m^3, 276 m and 3.3 m in Kampen, compared to 587 m^3, 441 m and 3.7 m in Puan Klent. Along both sides of the island, the time-averaged standard deviation in beach volume was relatively large, at ~10% of the mean. The alongshore variability in the sandbar location was larger in Kampen (57 m) than in Puan Klent (37 m), but please keep the difference in length of both shorelines in mind.

On the decadal timescale, no influence of the nourishments on the beach volume or sandbar crest location was observed, although responses to nourishments occurred on shorter timescales. For instance, the beach volume in Kampen (Figure 7a) increased notably after the beach nourishment of 1 000 000 m^3 in 1990. Thereafter, however, the beach volume was kept relatively constant with a nourishment in 2000 (460 000 m^3), followed by smaller nourishments (average of 140 000 m^3). We observed a high alongshore variability in beach volume in 1999 and 2000. A closer inspection of the data revealed that this was caused by the shoreface nourishment placed in 1996. After this shoreface nourishment, the sandbar initially

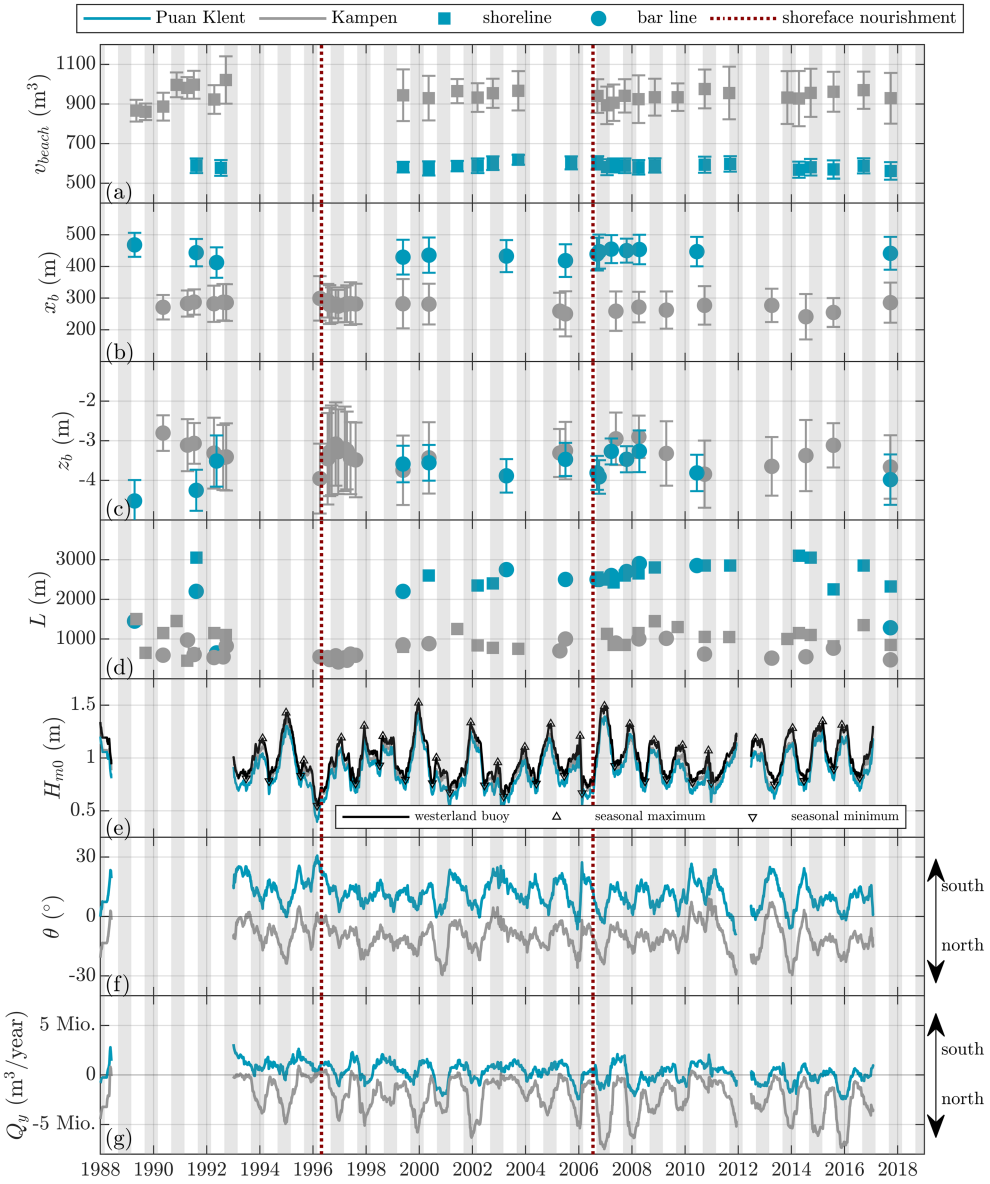

Figure 7. Temporal variability in mean and standard deviation of (a) beach volume, (b) bar line location and (c) bar line depth; (d) wavelength of alongshore variability in shoreline and bar line, seasonally varying; (e) spectral wave height at Westerland buoy (H13, black), nearshore Puan Klent (Hn, grey) and nearshore Kampen (Hn, blue); (f) wave angle of incidence; and (g) potential alongshore transport rates in Puan Klent and Kampen. Red dashed lines indicate the two studied shoreface nourishments. [Colour figure can be viewed at wileyonlinelibrary.com]

presented a more offshore and deeper location (Figures 7b and c). Thereafter, the sandbar quickly migrated onshore with significantly increased alongshore variability in the depth of the bar crest.

The bar crest location in front of Puan Klent presented a similar response to the shoreface nourishment of 2006, with a more offshore (439 m) and deeper location (−3.8 m). In the years that followed, however, the bar crest location remained relatively constant while the bar crest depth decreased at first and then remained constant. In the next subsection, we describe the response of the sandbars to these shoreface nourishments in more detail to gain more insight into the short-term behaviour of the sandbars on both island sides.

Figure 7d shows the smaller 3D length scale of the alongshore bar crest location in Kampen (mean of 670 m) compared to Puan Klent (mean of 2240 m). Furthermore, the 3D length scale in Puan Klent increased from approximately 2500 m to approximately 3000 m between 2000 and 2016 (Figures 8a and b). On average, the sandbar migrated with a speed of approximately 80 m year^{-1} in the southern direction. Since the two seaward-directed shoreline perturbations remained attached to the shoreward-directed sandbar horns, they were systematically coupled out-of-phase. The 3D length scale of the bar alongshore crest location in Kampen was generally smaller than the 3D length scale of the alongshore beach volume (mean of 1025 m). No phase coupling between the shoreline and the sandbar was thus observed in Kampen (Figures 8c and d). Figure 7e presents the seasonality in wave height, with more energetic waves during winter (maximum half-yearly H_{m0} between 0.96 and 1.52 m) and less energetic waves during summer (minimum half-yearly H_{m0} between 0.55 and 0.93 m). The seasonality in the wave climate also reflected on the wave angle of incidence. Figure 7f shows the seasonality and the difference in wave angle of incidence between Kampen and Puan Klent. In general, no clear seasonal effect of refraction was observed (Figure 7e). However, during storm events approaching from a south-westerly direction, wave heights could decrease significantly towards the northern

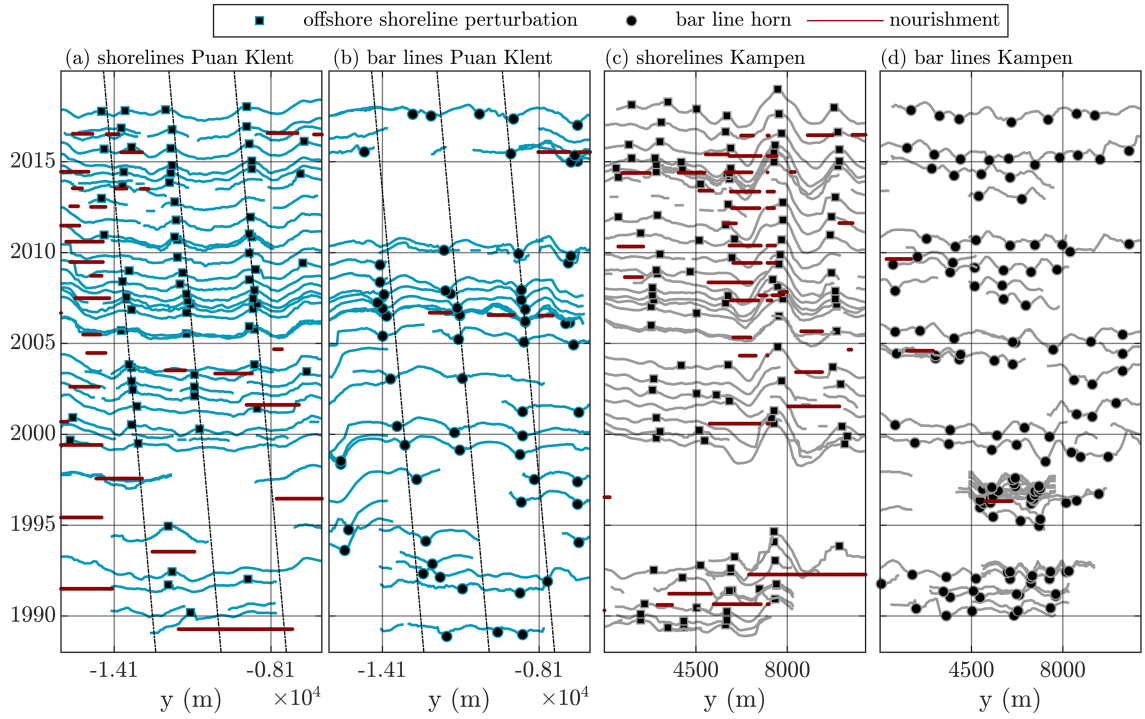

Figure 8. (a) Shorelines and (b) bar lines of Puan Klent. (c) Shorelines and (d) bar lines of Kampen. Red lines indicate beach nourishments in panels a and c, and shoreface nourishments in panels b and d. The dashed lines indicate shoreline and bar line migration of 80 m year^{-1} in Puan Klent, with separation distance of 2500 m. [Colour figure can be viewed at wileyonlinelibrary.com]

shoreline. Lastly, due to the combined effect of the seasonally varying wave height and angle, longshore transport rates [following Equation (1)] varied strongly between the seasons. Especially in Kampen, the combined effect of more energetic waves and larger southerly wave angles resulted in relatively large northward-directed transport rates of O(1 000 000 m^3 year^{-1}) in the winter season. In Puan Klent, a seasonal pattern was observed but magnitudes were significantly smaller at O(100 000 m^3 year^{-1}).

Short-term sandbar behaviour

This subsection presents short-term responses of the sandbars to the shoreface nourishments of 2006 and 1996 in Puan Klent and Kampen. This comparison indicates characteristic differences in the short-term behaviour of the sandbar systems. We describe the cross-shore (Figure 9) and longshore (Figure 10) response of the sandbars. Please note that the nourishments

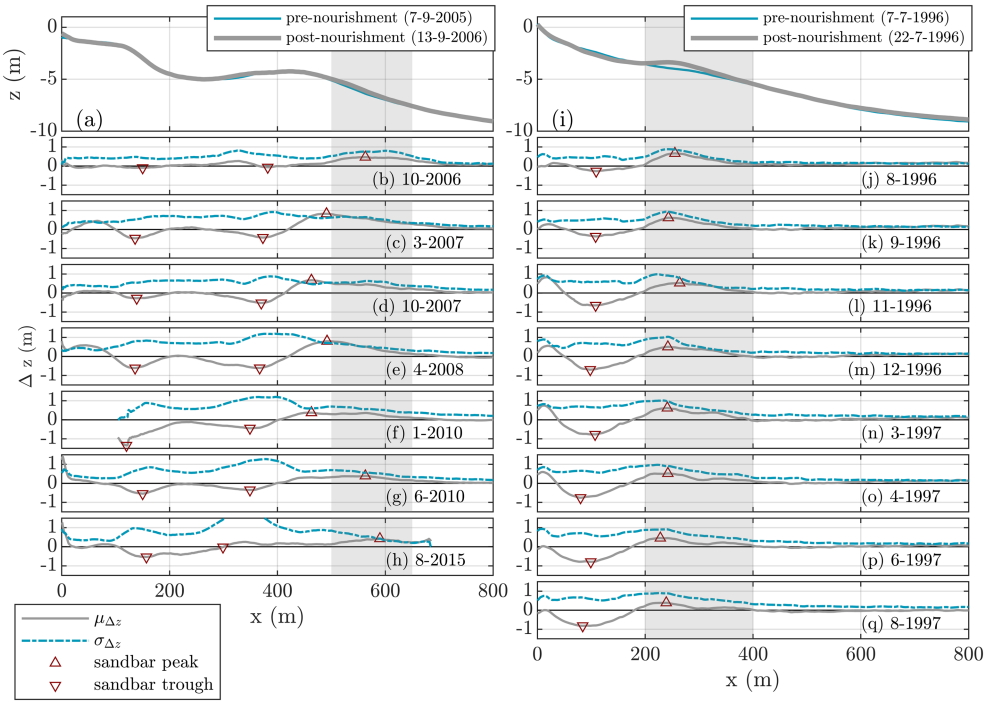

Figure 9. The cross-shore response of the sandbar in Puan Klent (a–h) and Kampen (i–q). Panels a and i show the pre- and post-nourishment profiles; panels b–h and j–q present the difference in the pre-nourishment profile. Alongshore standard deviation is shown by the dashed lines (--). The sandbar crest and trough are shown by the upward triangle (Δ) and downward triangle (∇). Grey shading indicates the initial nourishment location. [Colour figure can be viewed at wileyonlinelibrary.com]

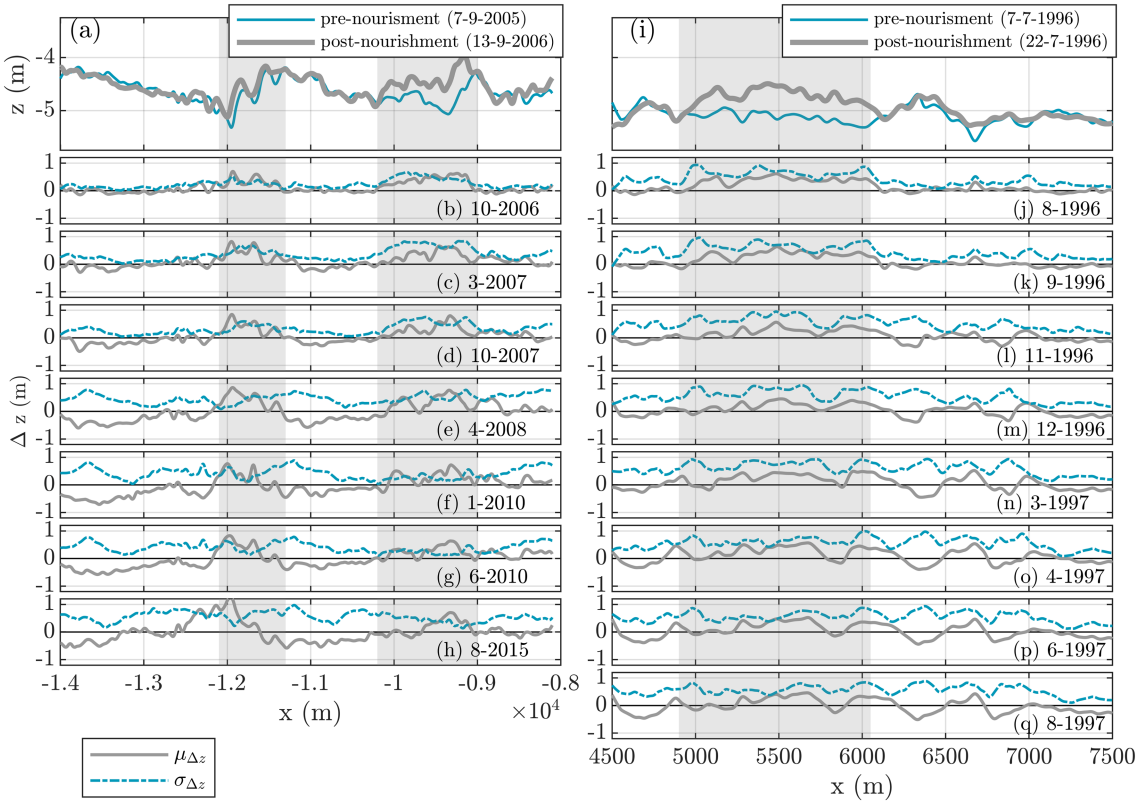

Figure 10. The longshore response of the sandbar in Puan Klent (a–h) and Kampen (i–q). Panels a and i show the pre- and post-nourishment profiles, panels b–h and j–q present the difference in the pre-nourishment profile. Cross-shore standard deviation is shown by the dashed lines (--). Grey shading indicates the initial nourishment location. [Colour figure can be viewed at wileyonlinelibrary.com]

were placed at different cross-shore locations (500–700 m in Puan Klent and 200–400 m in Kampen) and water depths (5–8 m in Puan Klent and 3.5–5 m in Kampen) (Figure 10).

The nourishment in Puan Klent attached to the existing sandbar after construction. The maximum alongshore-averaged amplitude increase was 0.45 m, 560 m from the shoreline (in October 2006, see Figure 9a). In Kampen, the nourishment formed into a new sandbar with maximum amplitude increase of 0.60 m, 250 m from the shoreline (in July 1996, see Figure 9i). Despite the differences in sandbar geometry and nourishment design, the sandbar amplified in combination with landward trough formation and shoreline advance (i.e. the breaker effect; Van Duin *et al.*, 2004). While the effect first showed in the winter season in Puan Klent, when mean daily wave heights became 1.52 m (Figure 9c), the effect occurred directly after construction in Kampen, when mean daily wave heights were 0.77 m (Figure 9i). Each winter season, the breaker effect was observed, while the shoreline eroded in the summer season in combination with onshore sandbar migration. Hence, the cross-shore breaker effect was observed for both sandbars, but the timing of the response depended on the depth of the sandbar and the wave height. We also observed a second landward trough forming in Puan Klent, thereby indicating two cross-shore locations with energetic wave breaking during winter (see Figures 9c and e).

In contrast to the cross-shore response, morphological changes in the longshore direction first showed in a later phase after the implementation of the nourishments. In Figures 10c (March 2007) and k (September 1996), for instance, the cross-shore mean differences in Puan Klent and Kampen were still coupled to the cross-shore standard deviation, thereby indicating that the cross-shore changes remained restricted to the initial nourishment location. In Kampen, cross-shore changes started occurring downstream of the nourishment location after a first period of energetic waves (mean daily wave height of 1.32 m) in November 1996. The observed behaviour can be identified as the leeside effect (Van Duin *et al.*, 2004). Leeside erosion was caused by the larger waves in combination with the larger wave angle (mean daily wave angle of −19°). The initiated morphological changes thereafter amplified and migrated in the downstream direction during the following winter (until March 1997). Limited changes were observed during the subsequent summer season. In Puan Klent, the first significant cross-shore changes outside the nourishment locations were observed after the winter of 2007–2008 (in April 2008). Energetic waves (mean daily wave height of 1.30 m) were measured in this period, but with near-zero wave angles (mean daily wave height of 2°). The observed changes were not resulting from the leeside effect but seemed related to the longshore migration of the sandbar.

In summary, while the nourishments did not affect the decadal behaviour of the sandbars, the analysis revealed short-term responses to shoreface nourishments in combination with events of larger waves and/or wave angles. These responses were dependent on the shoreface nourishment and on the varying wave conditions. The analysis also revealed that a second bar was present during winter in Puan Klent, while the Kampen sandbar, located in a shallower water depth, is more sensitive to causing leeside erosion during winter wave conditions.

Difference in wave climate between Sylt north and south

In general, the following differences in wave climate were observed between the northern and southern half of Sylt. The long-term average wave angle of incidence was Θ_N = 11.2° (northward) and Θ_S = −10.4° (southward), respectively. A

seasonality was present in the wave climate, with moderate conditions (H_{m0} = ~0.80 m) during the summer season (March to September) and energetic conditions (H_{m0} = ~1.30 m) during the winter season (October to February). The seasonality also reflected on the wave angle, with waves mainly from a north-westerly direction during summer and mainly from a south-westerly direction during winter (Figure 7f). Hence, the moderate summer waves approached the northern side with a near-zero angle (Θ_N ~ −10 to 10°) and the southern side with a larger wave angle from a northerly direction (Θ_S = 20–30°), while the energetic winter waves approached the southern side with a near-zero angle (Θ_S ~ −10 to 10°) and the northern side with a larger wave angle from a southerly direction (Θ_N = −20 to −30°).

Discussion

The geometry of the sandbar on the northern and southern halves of Sylt differed systematically and continuously on a decadal timescale. The difference was quantified for two coastal sections in particular, Kampen and Puan Klent. Kampen and Puan Klent represented the significant north–south differences in time-averaged beach slope (1:21 and 1:12), upper shoreface slope (1:30 and 1:45), cross-shore sandbar crest location (276 and 441 m), depth of sandbar crest (3.3 and 3.7 m), length scale of three-dimensionality of the sandbar crest (670 and 2240 m) and sandbar coupling to the shoreline (no coupling and out-of-phase coupling). In this section, we evaluate these differences and hypothesize how they are related to the difference in shoreline orientation along the curved shoreline, thereby focusing on the role of the local wave climate. Figure 11 provides a conceptual overview of the expected relations.

Sandbar behaviour on the northern half of Sylt

Due to refraction of the energetic winter waves towards the shoreline of the northern half of Sylt, we expected that this side of the island was more sheltered from energetic conditions from a south-westerly direction. On a seasonal scale, however, the data did not present this effect (Figure 7f). The steeper upper shoreface slope and the perhaps less energetic waves could explain the shorter sandbar distance from the shoreline and lower bar crest depth on the northern side. The shorter 3D length scales of the sandbar on the northern side furthermore suggest that its three-dimensionality formed during lower energetic conditions in summer, when wave angles were near zero. The formation of 3D sandbars during wave conditions with near-zero angles has been discussed extensively in the literature, thereby relating hydrodynamic forcing and sandbar characteristics in the same order of magnitude as observed on the northern half of Sylt (Van Enckevort *et al.*, 2004; Coco and Murray, 2007; Drønen and Deigaard, 2007; Thornton *et al.*, 2007; Price and Ruessink, 2011; Splinter *et al.*, 2011; Van de Lageweg *et al.*, 2013; Athanasiou *et al.*, 2018). Bar straightening, or a decrease in three-dimensionality of the sandbar, is often related to large rates of longshore sediment transport, when energetic waves approach with larger wave angles (Garnier *et al.*, 2013; Price *et al.*, 2014; Contardo and Symonds, 2015). On the northern side of Sylt, the transport rates become significant during winter (Figure 7g). These conditions can reduce the three-dimensionality of the sandbars as well as affect the coupling mechanisms to the shoreline (Rutten *et al.*, 2018). The fact that the sandbar was located closer to the shoreline and less pronounced suggests a lower transport rate necessary to be straightened. The observations therefore suggest that bar straightening of the sandbar, which forms during moderate summer conditions, occurs during energetic winter conditions. This dynamic may, in turn, lead to a too weak cell circulation to force sandbar–shoreline coupling. On the decadal timescale, the dynamics related to the sandbar can affect the longer-term evolution of the coastal profile, since the sandbar more effectively reduces incoming wave energy, which could explain the wider beach with milder slope on the northern side.

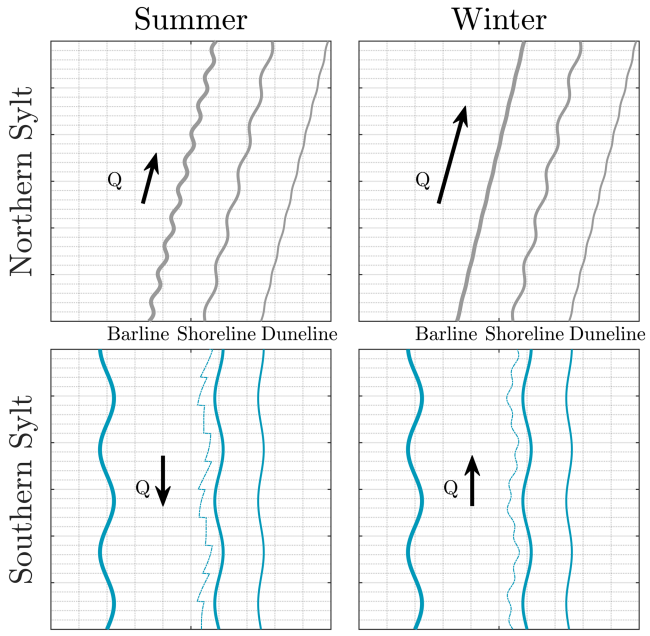

Figure 11. Schematic of observed differences in sandbar and shoreline behaviour and expected relation to wave climate, indicated by the longshore sediment transport rate *Q*. Not to scale. [Colour figure can be viewed at wileyonlinelibrary.com]

Sandbar behaviour on the southern half of Sylt

On the southern half, the moderate summer waves approach with a larger wave angle, from a northerly direction. The sandbar, however, located in a larger water depth, remained unaffected by these waves, which mainly affect the swash-backwash patterns on the low-tide terrace (Castelle *et al.*, 2007; Ruessink *et al.*, 2007). This dynamic was also observed in the sandbar response in Puan Klent to the shoreface nourishment in 2006, when the sandbar was persistent during the moderate summer conditions, while the morphology on the low-tide terrace was affected. The dynamic also explains the seasonal variation of the low-tide terrace characteristics, which has features of a 'Ridge-Runnel' state during winter and a 'Low-Tide Terrace' state during summer (see figure 6.3 in Lange, 2019). While the mild summer waves, approaching from the north, force the observed southward-directed skewness of the 'Ridge-Runnel' state, the near-zero-angle winter waves force the change towards the 'Low-Tide Terrace' state (Lipmann and Holman, 1990; Price and Ruessink, 2011).

The larger 3D length scales of the sandbar on the southern half, located more offshore and in a larger water depth, can be related to the milder upper shoreface slope, in combination with the more energetic conditions. Since the sandbar was persistent to the summer waves, it only became morphologically active during winter, as was identified during the two winter seasons after the shoreface nourishment in Puan Klent in 2006. The three-dimensionality of the sandbar therefore forms

during energetic conditions. An increasing sandbar three-dimensionality during energetic conditions has been observed previously (Rutten *et al.*, 2018). On the southern half of Sylt, these types of conditions occur during winter with near-zero angles, and occasionally during summer/autumn from larger wave angles from a northerly direction. Hence, the 3D patterns either form during the occasional summer/autumn storm conditions with larger wave angle of incidence (Calvete *et al.*, 2005), or the energetic winter waves with near-zero angles explain the relatively large 3D length scales of the sandbar compared to previous observations (Van Enckevort *et al.*, 2004).

Since the longshore sediment transport rates were generally significantly smaller on the southern half of Sylt, annual bar-straightening events did not occur. The energetic winter waves with near-zero angles do explain the out-of-phase coupling between the sandbar and the shoreline by means of a horizontal circulation cell (Castelle *et al.*, 2010a). Time-averaged sediment transport rates on the southern half were directed southward and could explain the observed southward migration of the coupled sandbar and shoreline (Figure 8a). Either the shoreline migrates southward during summer and the sandbar couples during winter, or the sandbar migrates southward during northerly summer/autumn storm events and is followed by the coupled shoreline during winter. The migration speed of the sandbar was observed to be approximately 80 m year^{-1}, which is in the same order of magnitude as for sand wave migration (Ashton and Murray, 2006b; Van Den Berg *et al.*, 2012). However, shoreline sand waves form during very large wave angles of incidence (Ashton and Murray, 2006a), while the observed shoreline migration is related to nearshore circulation processes. The persistent sandbar may affect the decadal evolution of the coastal profiles. Not only does the sandbar affect the alongshore variability of the shoreline, but the deeper-located sandbar is less effective in reducing wave energy, which can explain the narrower and steeper sloped beach on the southern half.

Applicability

While monitoring data sets of coastal profiles have been increasing over the last decades, their spatial and temporal resolution is often insufficient to study the morphological evolution of the sandbar in response to hydrodynamic events, such as storms. On Sylt, the coastal profiles were collected with alongshore intervals of 50 m, and the alongshore variability of the sandbar could be studied on decadal timescales. We observed significant and systematic differences in the decadal beach profiles and the behaviour of the sandbar along the curved coastline. While the present shape of Sylt has formed during the last centuries and was kept constant during the last decades (Ahrendt, 2001), we expect that the shoreline orientation in relation to the seasonality of the wave climate governs the nearshore morphology. We therefore expect that the observed differences remain as long as the island shape remains. The study implies that the local wave climate, in particular the combination of wave height and wave angle of incidence, is decisive for the decadal morphological evolution of nearshore sandbars and their effect on shorelines.

Conclusions

We studied 38 years of coastal profile measurements along the 34 km-long curved shoreline of Sylt in Germany. It was observed that, analogous to the shoreline curvature along Sylt, systematic and significant alongshore differences were present in the decadal coastal profile characteristics (i.e. the beach state). With an intermediate beach state, the profiles on the southern half presented features of the ridge-runnel (in summer) or low-tide terrace state (in winter), in combination with a rhythmic Gaussian-shaped sandbar further from the shoreline (on average 441 m). On the northern half, the beach profiles showed features of the transverse bar and rip state with a wider beach and a less pronounced sandbar, located closer to the shoreline (on average 276 m). A systematic difference in sandbar geometry was observed as well, with time-averaged 3D length scales of 2240 and 670 m on the southern and northern half, respectively. While the sandbar was coupled out-of-phase on the southern island half, no sandbar–shoreline coupling was observed on the northern island half.

We imply that the moderate summer waves, approaching the northern half of Sylt with near-zero angles, are responsible for the shorter 3D length scales of the sandbar. We found that the sandbar on the southern half of Sylt was persistent during these conditions, which did affect the low-tide terrace morphology. On the southern half, we therefore hold the energetic winter waves responsible for the formation of the larger sandbar distance, larger 3D length scales and observed out-of-phase coupling between sandbar and shoreline. Furthermore, we expect that during winter, when longshore transport rates are large on the northern half, the less-persistent sandbar straightened. On the southern half, the sandbar did not straighten because either waves were moderate (in summer) or wave angles were near zero (in winter). On the whole, our study has shown that small alongshore variations in wave climates, caused by the curvature of a coastline, may already affect the interaction between the hydrodynamic and morphological processes such that this leads to systematic and significant differences in the sandbar geometry on a decadal timescale.

Acknowledgements—The authors gratefully acknowledge the Coastal Authority of Schleswig-Holstein (LKN.SH), in particular Arfst Hinrichsen, for the provision of the wave buoy and coastal profile data, the discussion on the findings and the comments on the draft manuscript. We acknowledge Finn Mielck of the Alfred-Wegener-Institute (AWI) for sharing the grain size measurement. The study was funded through project STENCIL (Contract No. 03F0761) of the German Ministry of Education and Research (Bundesministerium für Bildung und Forschung or BMBF). We acknowledge the reviewers for their thoughtful comments on the manuscript.

Conflict of Interest

The authors declare no conflict of interest.

Data Availability Statement

The data that support the findings of this study are available from the LKN.SH with the permission of the LKN.SH. Restrictions apply to the availability of these data, which were used under license for this study.

References

Ahrendt K. 2001. Expected effect of climate change on Sylt island: results from a multidisciplinary German project. *Journal of Coastal Research* **18**: 141–146.

Ahrendt K, Koester R. 1996. An artificial longshore bar at the west coast of the island of Sylt/German Bight: first experiences. *Journal of Coastal Research* **12**(1): 354–367. https://www.jstor.org/stable/4298485?seq=1

Ashton AD, Murray AB. 2006a. High-angle wave instability and emergent shoreline shapes: 1. Modeling of sand waves, flying spits, and capes. *Journal of Geophysical Research: Earth Surface* **111**(4): 1–19. https://doi.org/10.1029/2005JF000422

Ashton AD, Murray AB. 2006b. High-angle wave instability and emergent shoreline shapes: 2. Wave climate analysis and comparisons to nature. *Journal of Geophysical Research: Earth Surface* **111**(4): 1–17. https://doi.org/10.1029/2005JF000423

Athanasiou P, de Boer W, Yoo J, Ranasinghe R, Reniers A. 2018. Analysing decadal-scale crescentic bar dynamics using satellite imagery: a case study at Anmok beach, South Korea. *Marine Geology* **405**: 1–11. https://doi.org/10.1016/j.margeo.2018.07.013

Blossier B, Bryan KR, Daly CJ, Winter C. 2016. Spatial and temporal scales of shoreline morphodynamics derived from video camera observations for the island of Sylt, German Wadden Sea. *Geo-Marine Letters* **37**: 111–123. https://doi.org/10.1007/s00367-016-0461-7

Calvete D, Dodd N, Falque A, van Leeuwen SM. 2005. Morphological development of rip channel systems: normal and near-normal wave incidence. *Journal of Geophysical Research* **110**: C10006. https://doi.org/10.1029/2004JC002803

Castelle B, Bonneton P, Dupuis H, Sénéchal N. 2007. Double bar beach dynamics on the high-energy meso-macrotidal French Aquitanian coast: a review. *Marine Geology* **245**: 141–159. https://doi.org/10.1016/j.margeo.2007.06.001

Castelle B, Ruessink BG, Bonneton P, Marieu V, Bruneau N, Price TD. 2010a. Coupling mechanisms in double sandbar systems. Part 1: patterns and physical explanation. *Earth Surface Processes and Landforms* **35**(4): 476–486. https://doi.org/10.1002/esp.1929

Castelle B, Ruessink BG, Bonneton P, Marieu V, Bruneau N, Price TD. 2010b. Coupling mechanisms in double sandbar systems. Part 2: impact on alongshore variability of inner-bar rip channels. *Earth Surface Processes and Landforms* **35**(7): 771–781. https://doi.org/10.1002/esp.1949

Castelle B, Marieu V, Bujan S, Splinter KD, Robinet A, Sénéchal N, Ferreira S. 2015. Impact of the winter 2013–2014 series of severe Western Europe storms on a double-barred sandy coast: beach and dune erosion and megacusp embayments. *Geomorphology* **238**: 135–148. https://doi.org/10.1016/j.geomorph.2015.03.006

CERC. 1984. *Shore Protection Manual (SPM)*. Coastal Engineering Research Center: Washington, D.C.

Coco G, Murray AB. 2007. Patterns in the sand: from forcing templates to self-organization. *Geomorphology* **91**: 271–290. https://doi.org/10.1016/j.geomorph.2007.04.023

Coco G, Calvete D, Ribas F, Falques A. 2020. Emerging crescentic patterns in modeled double sandbar systems. *Earth Surface Dynamics Discussions* **8**: 323–334. https://doi.org/10.5194/esurf-2019-70

Contardo S, Symonds G. 2015. Sandbar straightening under wind-sea and swell forcing. *Marine Geology* **368**: 25–41. https://doi.org/10.1016/j.margeo.2015.06.010

Dette, HH. 1998. Management of Beach Nourishment in an Open Sand System. In *proceedings of the 26th International Conference on Coastal Engineering*. https://doi.org/10.1061/9780784404119.231

Drønen N, Deigaard R. 2007. Quasi-three-dimensional modelling of the morphology of longshore bars. *Coastal Engineering* **54**: 197–215. https://doi.org/10.1016/j.coastaleng.2006.08.011

Falques A, Coco G, Huntley D. 2000. A mechanism for the generation of wave-driven rhythmic patterns in the surf zone. *Journal of Geophysical Research* **105**(C10): 24071–24087. https://doi.org/10.1029/2000JC900100

Galal EM, Takewaka S. 2011. The influence of alongshore and cross-shore wave energy flux on large- and small-scale coastal erosion patterns. *Earth Surface Processes and Landforms* **36**(7): 953–966. https://doi.org/10.1002/esp.2125

Garnier R, Falqués A, Calvete D, Thiébot J, Ribas F. 2013. A mechanism for sandbar straightening by oblique wave incidence. *Geophysical Research Letters* **40**(March): 2726–2730. https://doi.org/10.1002/grl.50464

Gijsman R, Visscher J, Schlurmann T. 2019. An assessment of beach nourishment lifetimes on Sylt in Germany. In *Proceedings of the 9th Short Course/Conference on Applied Coastal Research*.

Huisman B, Walstra D-J, Radermacher M, de Schipper M, Ruessink G. 2019. Observations and modelling of shoreface nourishment behaviour. *Journal of Marine Science and Engineering* **7**(3): 59. https://doi.org/10.3390/jmse7030059

Kroon A, Larson M, Möller I, Yokoki H, Rozynski G, Cox J, Larroude P. 2007. Statistical analysis of coastal morphological data sets over seasonal to decadal time scales. *Coastal Engineering* **54**(6–7): 477–491. https://doi.org/10.1016/j.coastaleng.2007.01.003

Lange L. 2019. *Foreshore Morphodynamics from Shore-Based Marine Radar*. Delft University of Technology: Delft.

Lipmann T, Holman R. 1990. The spatial and temporal variability of sand bar morphology. *Journal of Geophysical Research* **95**(C7): 11 575–11 590. https://doi.org/10.1029/JC095iC07p11575

LKN.SH. 2016a. Fachplan Kuestenschutz Sylt: Bisheriger Kuestenschutz - Sanderzatz.

LKN.SH. 2016b. Fachplan Kuestenschutz Sylt: Grundlagen - Hydrologie.

Mielck F. 2017. *Westerland_2017.xlsx*. Alfred-Wegener-Institute: Bremerhaven.

Price TD, Ruessink BG. 2011. State dynamics of a double sandbar system. *Continental Shelf Research* **31**(6): 659–674. https://doi.org/10.1016/j.csr.2010.12.018

Price TD, Ruessink BG. 2013. Observations and conceptual modelling of morphological coupling in a double sandbar system. *Earth Surface Processes and Landforms* **38**(5): 477–489. https://doi.org/10.1002/esp.3293

Price TD, Ruessink BG, Castelle B. 2014. Morphological coupling in multiple sandbar systems; a review. *Earth Surface Dynamics* **2**(1): 309–321. https://doi.org/10.5194/esurf-2-309-2014

Quartel S, Kroon A, Ruessink BG. 2008. Seasonal accretion and erosion patterns of a microtidal sandy beach. *Marine Geology* **250**: 19–33. https://doi.org/10.1016/j.margeo.2007.11.003

Ribas F, Falqués A, Garnier R. 2017. Nearshore sand bars. In *Atlas of Bedforms in the Western Mediterranean*, Guillén J, Acosta J, Chiocci FL, Palanques A (eds). Springer: Cham; 73–79. https://doi.org/10.1007/978-3-319-33940-5_13

Ruessink BG, Coco G, Ranasinghe R, Turner IL. 2007. Coupled and noncoupled behavior of three-dimensional morphological patterns in a double sandbar system. *Journal of Geophysical Research: Oceans* **112**(7): 1–11. https://doi.org/10.1029/2006JC003799

Rutten J, Dubarbier B, Price TD, Ruessink BG, Castelle B. 2019. Alongshore variability in crescentic sandbar patterns at a strongly curved coast. *Journal of Geophysical Research: Earth Surface* **124**(12): 2877–2898. https://doi.org/10.1029/2019JF005041

Rutten J, Ruessink BG, Price TD. 2018. Observations on sandbar behaviour along a man-made curved coast. *Earth Surface Processes and Landforms* **43**(1): 134–149. https://doi.org/10.1002/esp.4158

Splinter KD, Holman RA, Plant NG. 2011. A behavior-oriented dynamic model for sandbar migration and 2DH evolution. *Journal of Geophysical Research* **116**(April): 1–21. https://doi.org/10.1029/2010JC006382

Staudt F, Gijsman R, Ganal C, Mielck F, Wolbring J, Hass HC, Goseberg N, Schüttrumpf H, Schlurmann T, Schimmels S. 2019. The sustainability of beach nourishments: a review of nourishment and environmental monitoring practice. *Journal of Coastal Conservation* in review. https://doi.org/10.31223/osf.io/knrvw

Thornton E, Macmahan J, Sallenger A, Jr. 2007. Rip currents, megacusps, and eroding dunes. *Marine Geology* **240**: 151–167. https://doi.org/10.1016/j.margeo.2007.02.018

Van de Lageweg WI, Bryan KR, Coco G, Ruessink BG. 2013. Observations of shoreline–sandbar coupling on an embayed beach. *Marine Geology* **344**: 101–114. https://doi.org/10.1016/j.margeo.2013.07.018

Van Den Berg N, Falqués A, Ribas F. 2012. Modeling large scale shoreline sand waves under oblique wave incidence. *Journal of Geophysical Research: Earth Surface* **117**(3): 1–18. https://doi.org/10.1029/2011JF002177

Van Duin MJP, Wiersma NR, Walstra DJR, Van Rijn LC, Stive MJF. 2004. Nourishing the shoreface: observations and hindcasting of the Egmond case, The Netherlands. *Coastal Engineering* **51**: 813–837. https://doi.org/10.1016/j.coastaleng.2004.07.011

Van Enckevort IMJ, Ruessink BG. 2003. Video observations of nearshore bar behaviour. Part 1: alongshore uniform variability. *Continental Shelf Research* **23**(5): 501–512. https://doi.org/10.1016/S0278-4343(02)00234-0

Van Enckevort IMJ, Ruessink BG, Coco G, Suzuki K, Turner IL, Plant NG, Holman RA. 2004. Observations of nearshore crescentic sandbars. *Journal of Geophysical Research* **109**(6): 1–17. https://doi.org/10.1029/2003JC002214

Wright LD, Short AD. 1984. Morphodynamic variability of surf zones and beaches. *Marine Geology* **56**: 93–118. https://doi.org/10.1016/0025-3227(84)90008-2

